Materials Letters 382 (2025) 137932

Contents lists available at ScienceDirect

Materials Letters

journal homepage: www.elsevier.com/locate/matlet

Unveiling single-electron tunneling in nanogranular ultrathin films for sensor applications via hyperspectral conductive AFM

Hicham Bakkali [a,*], Manuel Dominguez [b]

[a] Materials Science and Engineering Area, ESCET, Universidad Rey Juan Carlos, C/Tulipán s/n, 28933 Móstoles, Madrid, Spain
[b] Departamento de Física de la Materia Condensada & IMEYMAT: Institute of Research on Electron Microscopy and Materials, University of Cadiz, E11510 Puerto Real, Cádiz, Spain

ARTICLE INFO

Keywords:
Nanogranular ultrathin films
Electrical characteristics
Conductive atomic force microscopy
Single-electron tunneling

ABSTRACT

This study maps the electrical behavior across a 7 × 7 μm^2 nanogranular ultrathin Pd-ZrO_2 film, revealing nonlinear I-V characteristics indicative of single-electron tunneling. Following the Coulomb blockade power law $I \sim (V - V_t)^{\xi}$ with a scaling exponent $\xi \approx 1.2$, these characteristics appear above the threshold voltage V_t. By modeling the nanogranular structure as a 1D array of multitunnel junctions, we demonstrate a linear relationship between V_t and tunnel channel length, allowing for a better understanding of nanoscale electrical properties and supporting the development of sensitive sensors.

1. Introduction

Thin films of nanogranular metals (NGMs), with metal nanoparticles randomly distributed in an insulating matrix, are important for studying quantum size interactions and electronic correlation effects in various applications [1,2]. The coupling degree between particles affects their electronic response, ranging from weak quantum coupling ($g < 1$, tunneling regime) to strong coupling ($g > 1$, metallic regime) [3–5]. The DC conduction mechanism in NGM thin films has been widely studied [6–9]. It has been established that for $g < 1$ and low electric fields, thermally activated tunneling dominates when interparticle distances are around one nanometer or less [10,11]. This is linked to the Coulomb blockade (CB) of small nanoparticles, where thermal energy k_BT must overcome the Coulomb charge energy $E_C^0 = \frac{e^2}{C}$ associated with each particle. The CB effect makes NGMs ideal for developing single electron-tunneling (SET) nanodevices, enabling the monitoring and manipulation of individual electron movement. They also facilitate the creation and tuning of nanostructured thin films for applications like single-electron memories [12] and microwave and infrared radiation detectors [13,14].

Two quantum conditions must be met to observe the CB effect: (i) the activation energy for transferring an electron between adjacent islands, $E_C^1 = \frac{e^2}{2C}$, must exceed thermal energy, requiring $E_C^1 \gg k_BT \approx 26$ meV at room temperature, and (ii) the tunneling resistance between the islands must be significantly greater than the quantum (Hall) resistance, i.e., $\gg \frac{h}{e^2} \approx 25.9$ kΩ.

For instance, several methods exist to create a Coulomb gap in nanoelectrodes near absolute zero [10], although CB can also occur at room temperature in various nanostructures with nanoparticles smaller than 10 nm [15–18]. Additionally, previous studies [16,19–22] have reported a power law relationship in the current–voltage (I-V) characteristics of a CB array in gold nanoparticle-based tunneling junctions separated by insulating barriers,

$$I \propto (V - V_t)^{\xi} \tag{1}$$

where V_t is the CB threshold voltage below which the current is zero, and ξ is a scaling exponent that depends on the dimensionality of the array. ξ values of 1 and 5/3 were predicted for quasidimensional (1D) and two-dimensional (2D) arrays, respectively. It is also shown that V_t (or the Coulomb gap) decreases linearly with increasing number of junctions [23]. In our previous work [10], we reported the CB differential conductivity scaling law using the combined parameter $(e|V|/k_BT)^{1/2}$ at low temperatures in a Pd-ZrO_2 NGM thin film with a narrow size distribution of 3 nm between interdigitated Au microcontacts. Here, we present local electrical conductivity measurements at ambient temperature for a similar sample using datacube conductive atomic force microscopy (DCUBE c-AFM) spectroscopy in contact mode [24,25].

2. Experimental

A Pd-ZrO_2 thin film, approximately 10 nm thick, was prepared as

* Corresponding author.
E-mail address: hicham.bakkali@urjc.es (H. Bakkali).

https://doi.org/10.1016/j.matlet.2024.137932
Received 22 July 2024; Received in revised form 8 December 2024; Accepted 21 December 2024
Available online 27 December 2024

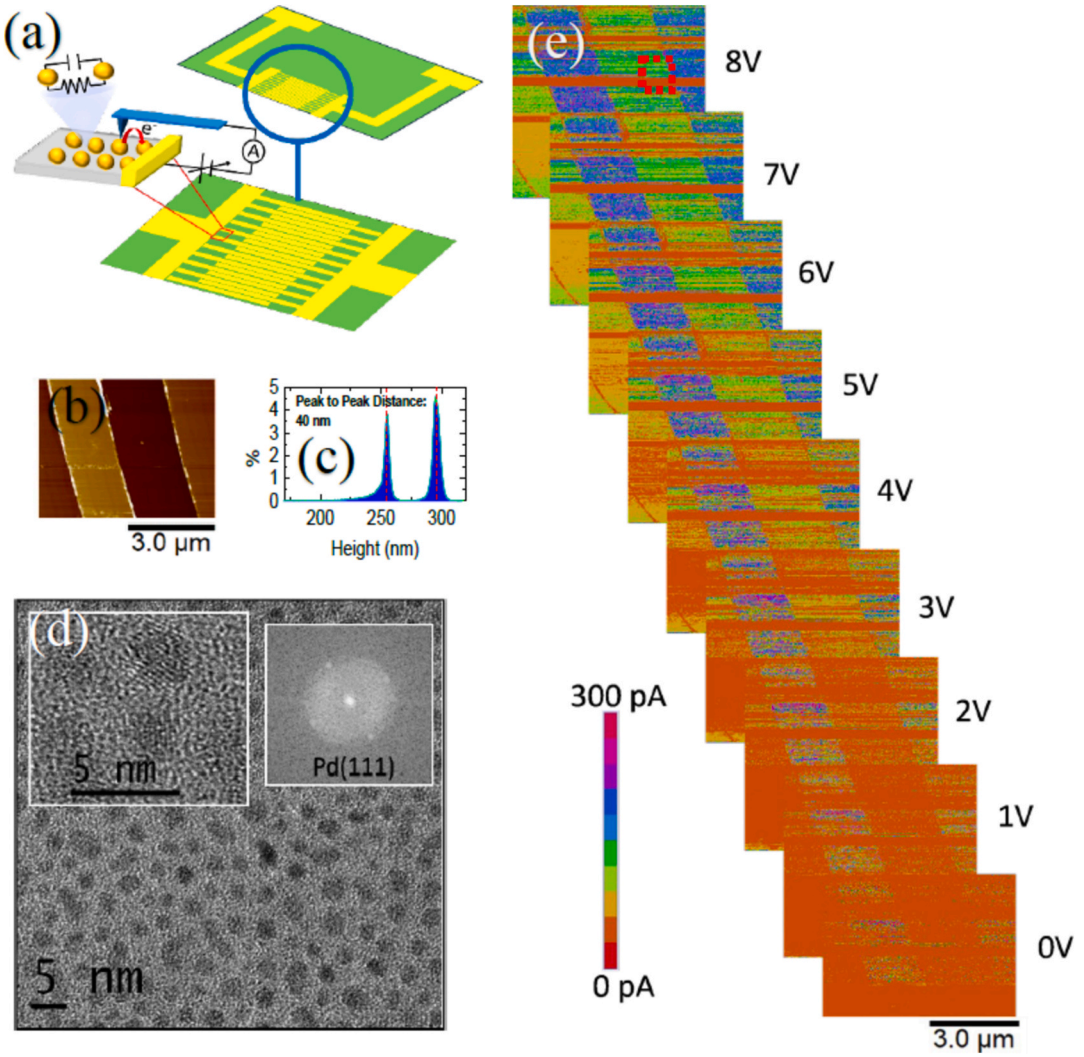

Fig. 1. (a) Schematic of interdigitated microcontacts, (b) topographic AFM image, and (c) height profile. Grain boundary regions are represented as parallel effective tunneling resistances and capacitances. (d) HR-TEM image of Pd-ZrO_2 NGM with 28 % Pd volume fraction, with insets showing a 600,000× image of NP clusters and NP diffraction pattern. (e) Nine representative current slices from a data cube at each bias voltage.

described in [10]. Local conductivity measurements were conducted using a Bruker Dimension Icon AFM with a ScanAsyst instrument in DCUBE c-AFM mode. The interdigitated Au reference electrode (Fig. 1a) was connected to the AFM metallic sample holder using silver paste, enabling current flow between the AFM tip and the electrodes. The interdigitated electrodes exhibited a bimodal height distribution (Fig. 1b, c), with an average height of 40 nm and a spacing of 2 μm, based on a Gaussian fit. A conductive diamond tip (AD-2.8-AS) analyzed a 7 × 7 μm^2 area at a resolution of 256 × 256 pixels. For DCUBE c-AFM acquisition, a force-distance cycle with a dwell segment was performed in the Z direction while the tip remained stationary in the XY plane. Each I-V spectrum was acquired during a 100 ms dwell segment as the sample bias voltage varied from −8 V to +8 V.

3. Results and discussion

Fig. 1d displays an HRTEM image of Pd-ZrO_2 with a 28 % Pd volume fraction. The average Pd nanoparticle size is 3 nm, with spacing under 1 nm. The left inset, at 600,000× magnification, shows narrow bands indicating the NPs' crystalline nature. The right inset provides atomic plane indexing, with a measured distance of about 0.22 nm, close to the 0.21 nm of the (111) plane in face-centered cubic (FCC) Pd nanocrystals. The sample bias range of −8 V to +8 V includes 209 data points, giving a 76.5 mV resolution between points in the I-V curves. This range yields 209 current slice images from the dwell segment. Fig. 1(e) shows nine representative current slice images of the same 7 × 7 μm^2 area in Pd-ZrO_2 thin films. Two distinct regions are visible: (i) a high-conductivity area near the interdigitated Au electrodes, where current flows perpendicular to the Pd-ZrO_2 layer (CPP geometry) between tip and electrode, and (ii) a low-conductivity area where current flows in-plane through the Pd-ZrO_2 NP sample. Below the threshold voltage ($V_t \approx 1.5$ V), current is minimal, but it rises sharply as bias increases.

We analyzed a region with uniform current intensities and a narrow current distribution (see dashed rectangle in Fig. 1e). Fig. 2 shows I-V curves from the DCUBE c-AFM dataset taken over a 10 × 10-pixel area. The I-V spectra reveal three threshold voltage groups (V_t), indicating three distinct tunneling channel lengths in the system [23]. All current spectra display a nonlinear dependence on sample bias (V_D), with nearly symmetrical characteristics. Additionally, differential conductance plots (dI_D/dV_D vs. V_D) derived from the I-V data show typical high-temperature parabolic behavior [10,19,26], suggesting that in-plane current flows through a CB array of tunnel junctions formed by gold nanoparticles separated by multiple tunneling barriers. To illustrate this, V_t values of 1.45, 3.38, and 4.43 V were calculated by averaging each

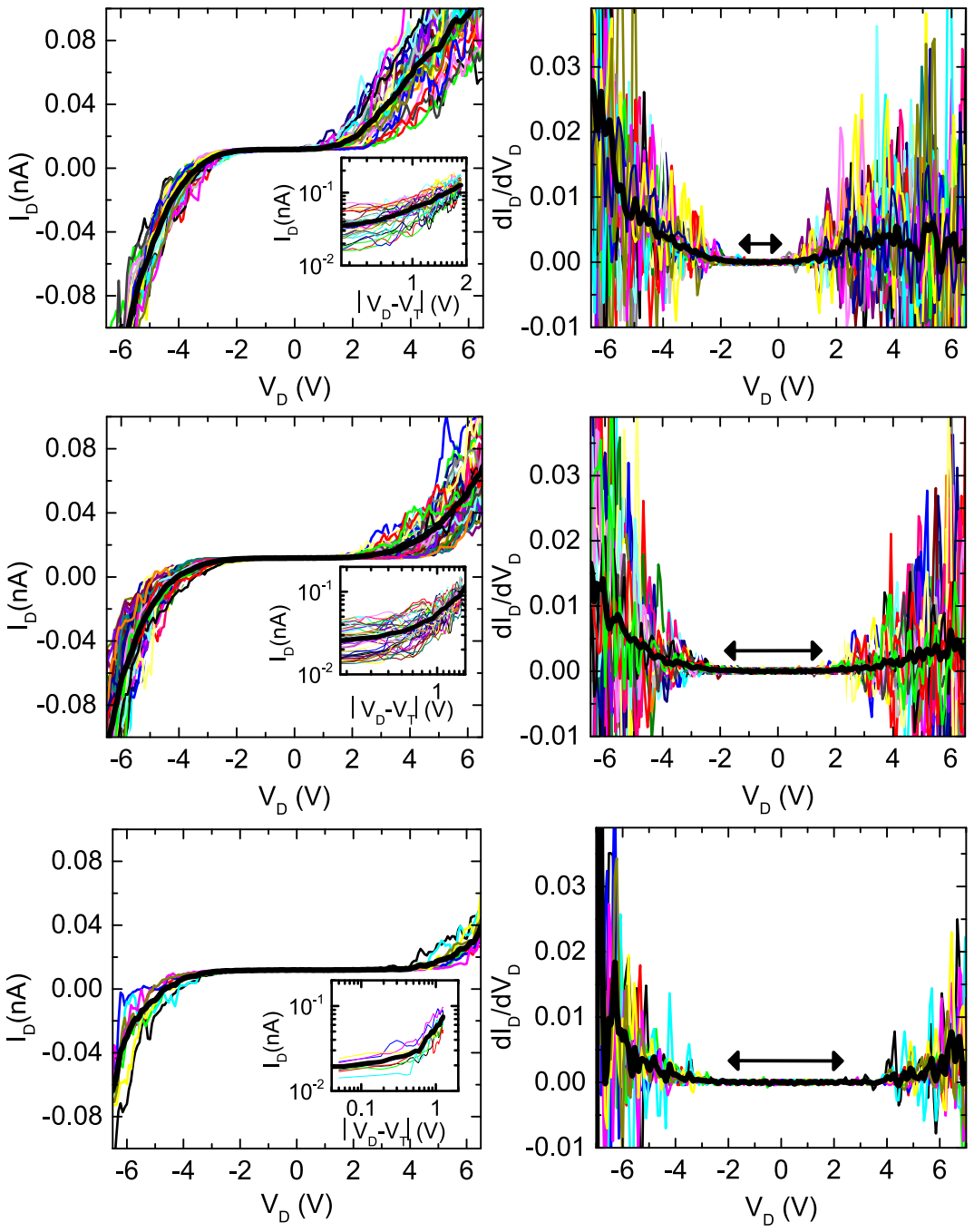

Fig. 2. I-V characteristics and log–log plot of differential conductance (dI_D/dV_D) vs. voltage at room temperature for sample groups with V_t values of 1.45, 3.38, and 4.43 V, from top to bottom. Data from 100 spectra taken in a 10 × 10-pixel area, with a resolution of 27.34 nm per pixel.

spectral set. Each V_t corresponds to the cumulative Coulomb gap of NPs along a transport path. Thus, I–V curves were plotted as $\ln(I_D)$ vs. $\ln|V_D - V_t|$ (Fig. 3), forming a straight line for $V > V_t$, confirming thermally assisted tunneling per Eq. (1). The alignment of curves for different V_t on a single line supports the CB scaling law. The slope of this line, with an exponent $\xi = 1.2$, suggests a 1D tunneling junction arrangement [22]. To assess junction number effects on Vt, I-V characteristics were measured at varying tip-to-electrode distances: L = 240, 480, 720, and 960 nm. Fig. 4 (left) presents four groups of I-V curves from the DCUBE c-AFM set, each representing a different distance. The effective current at each distance was calculated by averaging 30 I-V spectra per group (thick red curve). All I-V curves display nonlinear responses, indicating electron tunneling. V_t values were derived in Fig. 4 (right) by plotting $\ln(I_D)$ vs. $\ln(V_D)$ and finding the intersection of power-law fit lines near zero-current regions due to the CB effect [23]. The threshold voltage and channel length relationship suggests an increase in the CB gap with more tunneling channels, resulting in a linear increase in V_t as channel length increases. Here, CB follows the model [23].

4. Conclusions

We present an in-depth analysis of single-electron tunneling in nanogranular ultrathin Pd-ZrO_2 films using hyperspectral c-AFM, showing a CB effect at room temperature. The sample's I-V

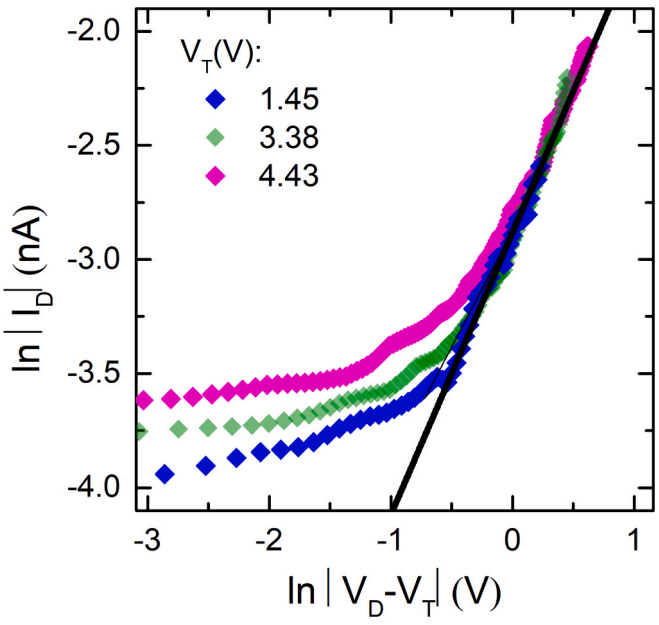

Fig. 3. Scaling plot of ln(I) versus $\ln(V_D - V_t)$. The slope of the linear fit yields an exponent ξ of 1.2.

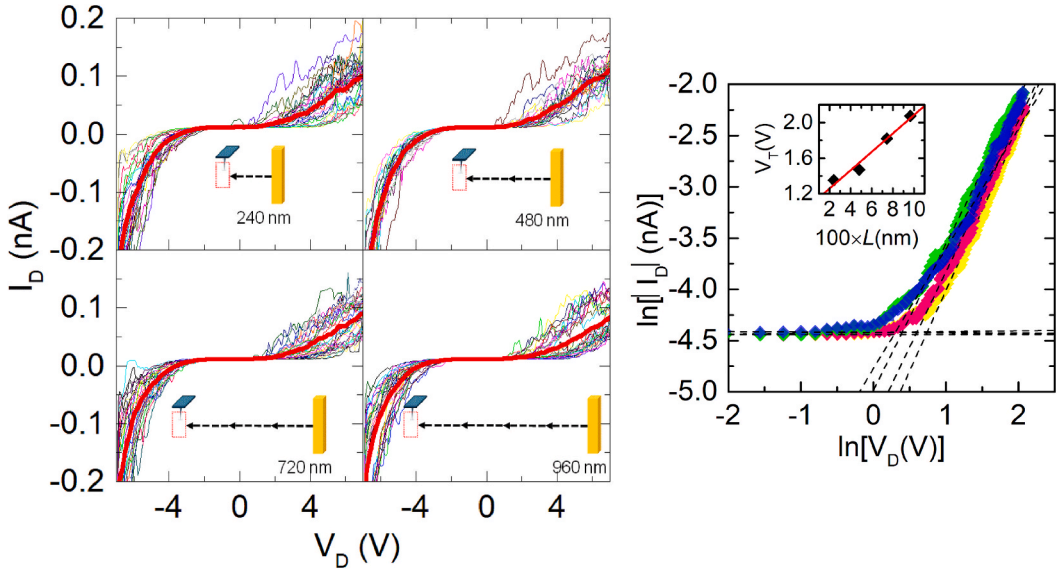

Fig. 4. Left: I-V curves for a sample with multiple channel lengths corresponding to tip-to-electrode distances of 240, 480, 720, and 960 nm. Thirty spectra are shown for each distance, arranged in a 6 × 5 pixel matrix. Right: ln(I) vs. ln(V) curves for L = 240, 480, 720, and 960 nm. The inset displays the linear relationship between Vt and L.

characteristics follow the power law $I \sim (V - Vt)^{\xi}$, with a scaling exponent $\xi \approx 1.2$, corresponding to a 1D multichannel junction arrangement. The Coulomb gap width increases linearly with the number of channel junctions, following $V_t \propto L$.

CRediT authorship contribution statement

H. Bakkali: Writing – review & editing, Writing – original draft, Visualization, Validation, Software, Methodology, Investigation, Formal analysis, Conceptualization. **M. Dominguez:** Writing – review & editing, Validation, Supervision.

Declaration of competing interest

The authors declare that they have no known competing financial interests or personal relationships that could have appeared to influence the work reported in this paper.

Acknowledgments

We would like to thank Dr M. Febvre (Bruker) for his support with the sample measurements. M.D. acknowledged the support by the Spanish "Ministerio de Ciencia, Innovación y Universidades" under project EQC2018-004704-P.

Appendix A. Supplementary data

Supplementary data to this article can be found online at https://doi.org/10.1016/j.matlet.2024.137932.

Data availability

No data was used for the research described in the article.

References

[1] M. Huth, *J. Appl. Phys.* 107 (2010) 113709.
[2] R. Sachser, F. Porrati, C.H. Schwalb, M. Huth, *Phys. Rev. Lett.* 107 (2011) 206803.
[3] I.S. Beloborodov, K.B. Efetov, A. Altland, F.W.J. Hekking, *Phys. Rev. B* 63 (2001) 115109.
[4] H. Bakkali, E. Blanco, S.E. Lofland, M. Domínguez, *New J. Phys.* 22 (2020) 083018.
[5] I.S. Beloborodov, A.V. Lopatin, V.M. Vinokur, K.B. Efetov, *Rev. Mod. Phys.* 79 (2007) 469–518.
[6] H. Bakkali, E. Blanco, M. Dominguez, M.B. de la Mora, C. Sánchez-Aké, M. Villagrán-Muniz, D.S. Schmool, B. Berini, S.E. Lofland, *Nanotechnology* 31 (2020) 445701.
[7] P. Sheng, B. Abeles, Y. Arie, *Phys. Rev. Lett.* 31 (1973) 44–47.
[8] R.W. Cohen, G.D. Cody, M.D. Coutts, B. Abeles, *Phys. Rev. B* 8 (1973) 3689–3701.
[9] X. Batlle, A. Labarta, J. Phys. D Appl. Phys. 35 (2002) 201.
[10] H. Bakkali, M. Dominguez, EPL (Europhys. Lett.) 104 (2013) 17007.
[11] S. Mitani, S. Takahashi, K. Takanashi, K. Yakushiji, S. Maekawa, H. Fujimori, *Phys. Rev. Lett.* 81 (1998) 2799–2802.
[12] L. Guo, E. Leobandung, S.Y. Chou, *Science* 1997 (275) (1979) 649–651.
[13] T. Hirano, T. Matsui, J. Kawarabayashi, T. Iguchi, *J. Nucl. Sci. Technol.* 45 (2008) 78–80.
[14] B. Jalali-Jafari, S. Lotkhov, A. Zorin, *Appl. Sci.* 6 (2016) 35.
[15] M. Khaje, H. Sedghi, H. Goudarzi, M.T. Ahmadi, S.S. Rahimian Koloor, M. Petrů, *Nanomaterials* 10 (2020) 835.
[16] G. Wang, H. Tanaka, L. Hong, Y. Matsuo, K. Niikura, M. Abe, K. Matsumoto, T. Ogawa, K. Ijiro, *J. Mater. Chem.* 22 (2012) 13691.
[17] P.U. Vivitasari, Y. Azuma, M. Sakamoto, T. Teranishi, Y. Majima, *Mater. Res. Express* 4 (2017) 024004.
[18] S. Willing, H. Lehmann, M. Volkmann, C. Klinke, *Sci. Adv.* (2017) 3.
[19] A.N. Aleshin, H.J. Lee, S.H. Jhang, H.S. Kim, K. Akagi, Y.W. Park, *Phys. Rev. B* 72 (2005) 153202.
[20] A.A. Middleton, N.S. Wingreen, *Phys. Rev. Lett.* 71 (1993) 3198–3201.
[21] H.E. Romero, M. Drndic, *Phys. Rev. Lett.* 95 (2005) 156801.
[22] A. Zabet-Khosousi, A.-A. Dhirani, *Chem. Rev.* 108 (2008) 4072–4124.
[23] M. Akai-Kasaya, Y. Okuaki, S. Nagano, T. Mitani, Y. Kuwahara, *Phys. Rev. Lett.* 115 (2015) 196801.
[24] A. Cui, P. De Wolf, Y. Ye, Z. Hu, A. Dujardin, Z. Huang, K. Jiang, L. Shang, M. Ye, H. Sun, J. Chu, *Nanotechnology* 30 (2019) 235701.
[25] P. De Wolf, Z. Huang, B. Pittenger, A. Dujardin, M. Febvre, D. Mariolle, N. Chevalier, T. Mueller, *Micros Today* 26 (2018) 18–27.
[26] A. Vilan, *PCCP* 19 (2017) 27166–27172.